

Performance of tubular actuators constructed with dielectric elastomer materials

Chengguang Zhang(张成光)

Citation: Chin. Phys. B, 2025, 34 (**7**): 074501. DOI: 10.1088/1674-1056/add007
http://cpb.iphy.ac.cn; http://iopscience.iop.org/cpb

What follows is a list of articles you may be interested in

A modified heuristics-based model for simulating realistic pedestrian movement behavior

Wei-Li Wang(王维莉), Hai-Cheng Li(李海城), Jia-Yu Rong(戎加宇), Qin-Qin Fan(范勤勤), Xin Han(韩新), and Bei-Hua Cong(丛北华)

Chin. Phys. B, 2022, 31 (**9**): 094501. DOI: 10.1088/1674-1056/ac65f8

Effect of the Al/O ratio on the Al reaction of aluminized RDX-based explosives

Qian Zhao(赵倩), Jian-Xin Nie(聂建新), Wei Zhang(张伟), Qiu-Shi Wang(王秋实), Qing-Jie Jiao(焦清介)

Chin. Phys. B, 2017, 26 (**5**): 054502. DOI: 10.1088/1674-1056/26/5/054502

Nonlinear control of spacecraft formation flying with disturbance rejection and collision avoidance

Qing Ni(倪庆), Yi-Yong Huang(黄奕勇), Xiao-Qian Chen(陈小前)

Chin. Phys. B, 2017, 26 (**1**): 014502. DOI: 10.1088/1674-1056/26/1/014502

Discrete element crowd model for pedestrian evacuation through an exit

Peng Lin(林鹏), Jian Ma(马剑), Siuming Lo(卢兆明)

Chin. Phys. B, 2016, 25 (**3**): 034501. DOI: 10.1088/1674-1056/25/3/034501

Reactionless robust finite-time control for manipulation of passive objects by free-floating space robots

Guo Sheng-Peng (郭胜鹏), Li Dong-Xu (李东旭), Meng Yun-He (孟云鹤), Fan Cai-Zhi (范才智)

Chin. Phys. B, 2014, 23 (**5**): 054502. DOI: 10.1088/1674-1056/23/5/054502

Performance of tubular actuators constructed with dielectric elastomer materials

Chengguang Zhang(张成光)[1,2,†]

[1] *School of Mechanical and Electrical Engineering, Zhoukou Normal University, Zhoukou* 466001, *China*
[2] *School of Mechatronics, Harbin Institute of Technology, Harbin* 150001, *China*

(Received 15 January 2025; revised manuscript received 21 April 2025; accepted manuscript online 24 April 2025)

Soft underwater swimming robots driven by smart materials show unique advantages in ocean exploration, such as low noise, high flexibility and good environmental interaction ability. The dielectric elastomer (DE), as a new kind of soft intelligent material, has the characteristics of a low elastic modulus, large deformation range, high energy density and fast response speed. DE actuator (DEA) drive systems use the deformation characteristics of dielectric materials to drive the mechanical system, which has become a research hotspot in the field of soft robots. In this paper, a tubular actuator based on DEs is designed and its performance is studied. Firstly, the structure and driving process of a DEA are described, and a tubular DEA is designed. Studying the elongation ratio of the DEA pre-stretching shows that when the axial elongation ratio is 3 times and the circumferential elongation ratio is 4 times, the maximum deformation effect can be obtained under voltage excitation. At a voltage of 6.0 kV, a single pipe section DEA achieves a bending angle of 25.9° and a driving force of 73.8 mN. Secondly, the effect of the DEA series on the bending angle and response characteristics is studied. The experimental results show that the maximum bending angle of the three joint actuators in series can reach 59.3° under 6.0 kV voltage, which significantly improves the overall bending performance. In addition, the truncation frequency of the drive module after the series is increased to 0.62 Hz, showing better frequency response capability. The excellent performance of the pipe joint actuator in its bending angle, response characteristic and driving force is verified.

Keywords: dielectric elastomer (DE), tubular actuator, series, soft robot

PACS: 45.40.Ln, 47.54.Jk, 61.41.+e, 77.84.–s

DOI: 10.1088/1674-1056/add007 **CSTR:** 32038.14.CPB.add007

1. Introduction

The demand for underwater robots in marine biological and ecological investigations, seabed exploration, and the maintenance and inspection of aquatic equipment has increased. With advancements in science and technology, underwater swimming robots have attracted considerable attention from researchers.[1,2] At present, most underwater robots adopt spiral propulsion mechanisms. Highly precise control and fast swimming speeds can be achieved for rigid robot fishes driven by motors. However, because the screws rotate underwater, these robots face many challenges, such as high noise, large structures and inefficiency. Moreover, various problems affect the environment, such as interactions with marine life. Most fish-type robots reproduce the swimming movements of fish through motors and cranks, which are characterized by high body stiffness. It is difficult to reproduce the original soft movements of organisms, and the propulsion performance of organisms may not be sufficiently reproduced.[3] Previous works have attempted to address these issues by introducing soft robots with actuators and structures constructed based on flexible materials.[4] Bionic fish robots with excellent propulsion speed and agility can also be developed to address these issues. Soft robots made of flexible materials have several advantages, such as silent driving mechanisms, simplified body structures, high flexibility and high environmental adaptability.[5,6] In addition, soft robots can be used not only for underwater inspection and environmental monitoring but also as an experimental platform for studying the swimming mechanisms of fish.[7,8]

The dielectric elastomer (DE) actuator (DEA) is a kind of intelligent soft material with an electrical response function that is polarized at high voltages. A DEA typically has a 'sandwich' structure, consisting of a dielectric film and flexible electrodes that expand when stimulated by voltage. DEAs have many advantages, such as lightweight structures, large driving strain and fast response speeds. Although the excitation voltage usually reaches thousands of volts, the current is very small, which means that a small commercial battery module can meet the long-term operation needs of the robot. In addition, DEAs are suitable as driving materials for underwater swimming robots because of their low noise, near-water density and inherent transparency.

Pfeil attached a cylindrical DEA to an internal holding structure and designed a bionic worm-like crawling robot based on a DEA.[9] Xing *et al.* designed a manipulator composed of five DEA modules. Each module is composed of a spatially closed tubular structure, which has a large deforma-

[†]Corresponding author. E-mail: zhangchengguang@126.com

© 2025 Chinese Physical Society and IOP Publishing Ltd. All rights, including for text and data mining, AI training, and similar technologies, are reserved.

tion ability.[10] Almanza *et al.* proposed a heart transplantation treatment method based on a DE aorta and developed a cylindrical DEA to enhance the circulatory work of the heart by reducing the deformation of the systolic aorta and increasing the recompressive force of the diastolic aorta.[11] Liu *et al.* used a Coralzon metal spring as the compliant electrode of a cylindrical DEA. With the axial elongation of the tubular DEA, the flexible electrode of the metal spring kept conducting electricity without increasing stiffness.[12] Martinez *et al.* proposed an improved scheme for enhancing the aorta based on a DEA. The actuator is a multi-layer tubular DEA acting on the internal pressure of the blood. When activated in sync with the heart, the DEA provides energy and limits the load on the left ventricle.[13] Wang *et al.* developed a self-sensing mechanism for a DEA that does not require the use of an external device to measure displacement.[14]

In this study, a tube joint actuator based on a DE was successfully designed and manufactured. Based on the constitutive properties of DE materials, a theoretical model under the mechanoelectric coupling was constructed. The maximum output torque of the software driver based on the principle of minimum energy has a strict positive correlation with its bending angle under static equilibrium. The configuration of the pipe joint actuator was innovatively proposed. It was verified that the annular structure can effectively transform into three-dimensional bending deformation under electric field excitation. At the level of structural design, the regulation law of the performance of the actuator by a predrawing process is discussed. The synergistic effects of the axial and circumferential elongation ratio on the polarization and mechanical properties of dielectric films were systematically investigated by designing an orthogonal prestretching experimental platform. The coupling test of the single pipe actuator was carried out to verify its nonlinear response characteristics. Further, the modular series design verified the unique advantages of the series structure in extending the working frequency band.

2. DE driving principle

When a DE is used as an actuator in a soft robot fish, the actuator acts as a parallel plate capacitor. The two surfaces of the DE are coated with flexible electrodes. A voltage is applied between the two electrodes, and the opposite charges distributed on the surface electrodes on the two sides attract each other, resulting in an attractive force, known as the Maxwell force. The DEA is an actuator developed by Pelrine *et al.*[15] Its structure is very simple and consists of flexible electrodes made of DE materials. The DE driving principle is shown in Fig. 1.

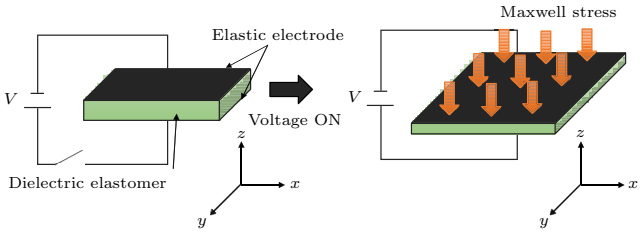


Fig. 1. DE driving principle.

Under Maxwell stress, the charges attract each other, and the elastomer compresses vertically and stretches horizontally, resulting in deformation. Compared with existing piezoelectric actuators and electrostatic actuators, the DEA can deform more. In addition, elastomer materials and flexible electrodes can easily be obtained. Moreover, because of its simple structure, arbitrary structures can be made with DEAs.

DEs are different from ordinary elastomers because the stress and deformation have a strong nonlinear relationship. These materials are called superelastic materials, and their elastic properties are expressed by the strain energy function W,

$$p_{ij} = \frac{\partial W}{\partial s_{ij}}, \tag{1}$$

where p represents the stress and s represents the strain.

The stress tensor is used to represent the three-dimensional stress and strain, and this tensor is shown in Fig. 2.

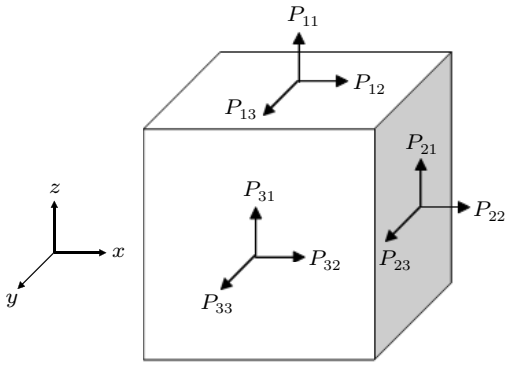


Fig. 2. Definition of the stress tensor.

The strain energy function W is a function of the Cauchy–Green deformation tensor c, which is expressed as a function of the invariants of strains I_1, I_2, and I_3. The strain energy function W can be expressed using the Yeoh model as follows:[16]

$$W = c_{10}(I_1 - 3) + c_{20}(I_1 - 3)^2 + c_{30}(I_1 - 3)^3, \tag{2}$$

where c_{10}, c_{20}, and c_{30} are experimentally obtained coefficients. I_1 can be expressed using the stretch ratio λ_i ($i = 1$, 2, 3)

$$I_1 = \lambda_1^2 + \lambda_2^2 + \lambda_3^2. \tag{3}$$

The stretch ratio λ_i represents the length after deformation in the direction of the principal axis divided by the length before deformation

$$\lambda_1 = 1 + s_i, \tag{4}$$

where s_i represents the distortion.

When the DE is compressed, the overall volume remains unchanged, and the relationship among the DE elongation ratios can be expressed as follows:

$$\lambda_1^2 \lambda_2^2 \lambda_3^2 = 1. \tag{5}$$

3. Driving principle

The driving process of the DE refers to the process of mechanical motion resulting from the change in the volume of the DE under the action of an electric field.[17] When a driving voltage is applied to the DE, the DE can be regarded as a flexible variable capacitor. Since the positive and negative charges attract each other, the electrodes on both sides of the DE base film create Maxwell stress, which squeezes the DE base film. Since the DE material has an incompressible volume, the DE base film becomes thinner after being subjected to Maxwell stress, resulting in an increase in the area of the DE.[18] When the voltage is removed, the DE rapidly shrinks because of its elastic properties and regains its original shape.

When a voltage is applied to the electrodes on both sides of the DE, the Maxwell stress p must be considered, which is formulated as follows:[19]

$$-Ap\,\mathrm{d}z = \mathrm{d}W, \tag{6}$$

where A represents the cross-sectional area in the xy plane and $\mathrm{d}W$ represents the work performed within a small interval $\mathrm{d}z$.

The capacitance C can be expressed as follows:

$$C = \frac{\epsilon_0 \epsilon_\mathrm{r} A}{z}. \tag{7}$$

The electric energy U_e depends on the charge Q as follows:

$$U_\mathrm{e} = \frac{zQ^2}{2\epsilon_0 \epsilon_\mathrm{r} A}, \tag{8}$$

where ϵ represents the dielectric constant of the vacuum and ϵ_r represents the dielectric constant of the insulator.

The change in the electric energy $\mathrm{d}U_\mathrm{e}$ is calculated as follows:

$$\mathrm{d}U_\mathrm{e} = \left(\frac{Q}{C}\right)\mathrm{d}Q + U_\mathrm{e}\left[\left(\frac{1}{z}\right)\mathrm{d}z + \left(\frac{1}{A}\right)\mathrm{d}A\right]. \tag{9}$$

If the charge remains unchanged, $\mathrm{d}Q = 0$, and the following formula is valid:

$$\mathrm{d}U_\mathrm{e} = U_\mathrm{e}\left[\left(\frac{1}{z}\right)\mathrm{d}z - \left(\frac{1}{A}\right)\mathrm{d}A\right]. \tag{10}$$

The following formula holds if the volume of the elastomer remains constant:

$$A\,\mathrm{d}z + z\mathrm{d}A = 0, \tag{11}$$

$$\mathrm{d}W = 2U_\mathrm{e}\left(\frac{1}{z}\right)\mathrm{d}z = -2U_\mathrm{e}\left(\frac{1}{A}\right)\mathrm{d}A. \tag{12}$$

According to Eqs. (6) and (12), we obtain

$$p = \frac{2U_\mathrm{e}}{Az}. \tag{13}$$

U_e can also be expressed as follows:

$$U_\mathrm{e} = \frac{1}{2}\epsilon_0 \epsilon_\mathrm{r} A z \left(\frac{V}{z}\right)^2 = \frac{1}{2}\epsilon_0 \epsilon_\mathrm{r} A z E^2, \tag{14}$$

where E represents the electric field.

By substituting Eq. (14) into Eq. (13), we obtain

$$p = \epsilon_0 \epsilon_\mathrm{r} E^2 = \epsilon_0 \epsilon_\mathrm{r}\left(\frac{V}{z}\right)^2. \tag{15}$$

4. Tubular DEA

4.1. Design of the tubular DEA

Although a good bending angle can be achieved with a rolling DEA, when multiple layers need to be wound together, the elastomer area must be large, and it is difficult to maintain a uniform thickness in the prestretched state. Moreover, the pattern electrodes must be correctly overlapped when wound. In a tubular DEA — the smallest rolled DEA structure — only one winding layer is included. The structure of the tubular DEA is shown in Fig. 3.

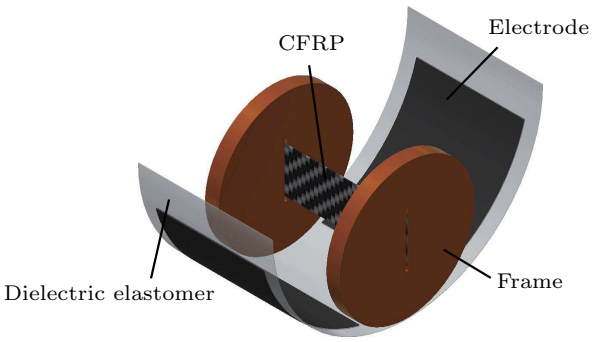


Fig. 3. The structure of the tubular DEA.

The tubular DEA consists of circular frames for winding the elastomer and a central elastic plate connecting the two frames; it is made by coating electrodes with carbon powder on a prestressed elastomer and then winding the electrodes around the circular frame. The CFRP, which is rigid and flexible, is chosen as the central elastic plate to maintain the compressive stress and increase bending in the horizontal direction.

4.2. DEA performance with prestretching

Prestretching can improve the performance of the actuator, especially when prestretching the actuator along the *x*- and *y*-axes with different stretch ratios, and larger deformations can be generated in the direction with smaller elongation ratios.[20] In this study, the elongation ratios of the DEs in the *x*-axis direction were 2:3, 2:4, and 2:5, and the elongation ratios of the DEs in the *y*-axis direction were 3:4 and 3:5. The drive of DEA requires high voltages above 1 kV, so high-voltage amplifiers are used. The high-voltage amplifier is a PS500 from Stanford Research Systems. A sinusoidal voltage with an amplitude of 3–5 kV and a frequency of 0.1 Hz was applied to the actuator. The initial electrode widths along the *x*- and *y*-axes and the maximum voltage were measured according to the image of the moving actuator, and the deformation was calculated according to the elongation. The relationships between the voltage applied via the asymmetric prestretching process and the deformation in each axial direction are shown in Fig. 4.

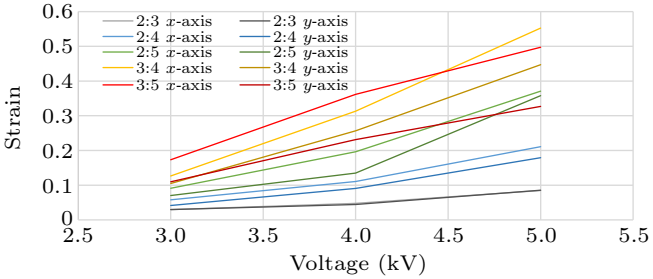


Fig. 4. Relationships between the voltage applied via the asymmetric prestretching process and the deformation in each axial direction.

For each stretch ratio, the distortion in the *x*-axis direction, with a smaller stretch ratio, was always greater than that in the *y*-axis direction. The distortion was greatest when the elongation ratio was 3:5. A similar elongation ratio of 3:4 was also considered in the asymmetric prestretching process. In all cases, the deformation was greater in the *x*-axis direction. At the same elongation ratio, the result with the greatest distortion demonstrates the effect of resilience because resilience hinders the driving process. When making a tubular DEA, to increase the bending angle, the deformation in the axial direction should be increased; thus, a 3:4 axial to circumferential elongation ratio was chosen.

4.3. Rigidity of the elastic plates

When a tubular DEA is constructed, the rigidity of the CFRP central elastic plate is a very important parameter. Therefore, the length, width and thickness of the CFRP were studied.

First, regarding the CFRP thickness, when the thickness t was 0.1 mm, the rigidity was insufficient, and the component was flattened because of the resilience of the material. When the thickness t was 0.3 mm, the rigidity of the material was high, and a sufficient bending angle could not be obtained. Therefore, the thickness of the CFRP was chosen to be $t = 0.2$ mm.

When the length l of the CFRP was short, the displacement and deformation of the tubular DEA were small. When the length l of the CFRP was long, a depression was observed in the center of the DE film, which affects the prestretching effect. Therefore, to prevent depressions in the DE material, various combinations of the length l and width w of the CFRP were investigated. The bending angle for each CFRP parameter combination at each voltage is shown in Fig. 5.

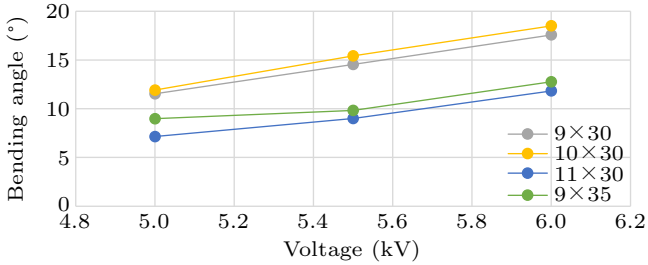


Fig. 5. Bending angle for each CFRP parameter combination with increasing voltage.

A sinusoidal voltage with an amplitude of 5.0 kV, 5.5 kV, or 6.0 kV, a frequency of 0.1 Hz and a phase difference of 180° were applied to the tubular DEA, and the bending angle of the actuator was measured.

A comparison of the results of actuators 9×30 and 9×35 reveals that the maximum bending angle was achieved with a CFRP with a length of 30 mm. In terms of the CFRP width, when the CFRP width was 10 mm, the maximum bending angle of the actuator was reached, and when the CFRP width was 9 mm or 11 mm, the bending angle of the actuator was reduced. Owing to the slight distortion of the DE due to the prestretching process, the left and right sides of the tubular actuator were not perfectly symmetrical. When the rigidity of the CFRP was low, the initial bending angle of the actuator was high owing to distortion effects. In contrast, when the CFRP stiffness was large, it was difficult to distort and deform the DE, reducing the initial bending angle of the actuator. Therefore, to reduce the initial bending angle of the actuator and improve the bending performance, the width of the CFRP was selected as 10 mm.

4.4. Circular frame

As the support structure of the tubular DEA, the size and shape of the circular frame also have an influence on the performance of the actuator. From the perspective of biological imitation, the diameter of the circular frame is 30 mm, which is equal to the diameter of the ordinary electric eel; the thickness of the circular frame is 3 mm, which is sufficiently thick to attach the medium-size elastomer material. Figure 6 shows

the CFRP parameters of the final DEA and circular frame. The size of the DEA is shown in Table 1. The final tubular DEA is shown in Fig. 7.

Table 1. Size of the pipe section of the DEA. l represents the length of the CFRP; w represents the width of the CFRP; t represents the thickness of the CFRP; d represents the diameter of the circular frame, and s represents the thickness of the circular frame.

Axial prestretch	Tangential prestretch	l (mm)	w (mm)	t (mm)	d (mm)	s (mm)
Extension ratio four	Extension ratio three	30	10	0.2	30	3

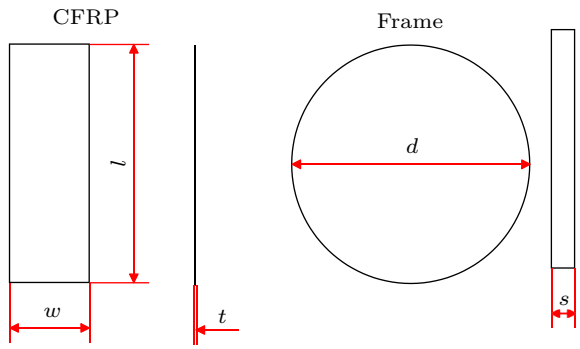


Fig. 6. Schematic diagram of the pipe section of the actuator.

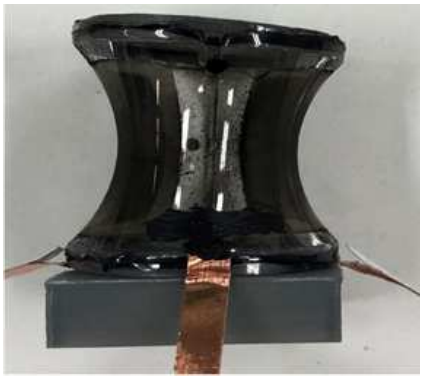


Fig. 7. The tubular DEA.

4.5. Performance evaluation of the tubular DEA

To study the driving characteristics of the tubular DEA, the bending angle, response characteristics, generating force and other aspects were experimentally investigated.

4.5.1. Measurement of the bending angle

To study the output of the tubular DEA, the relationship between the applied voltage and the bending angle of the tubular DEA was studied. A sinusoidal voltage with an amplitude of 1.0–6.0 kV, a frequency of 0.05 Hz and a phase difference of 180° was applied to the tubular DEA, and the bending angle of the actuator was measured. The maximum bending angle of the tubular DEA with increasing applied voltage is shown in Fig. 8.

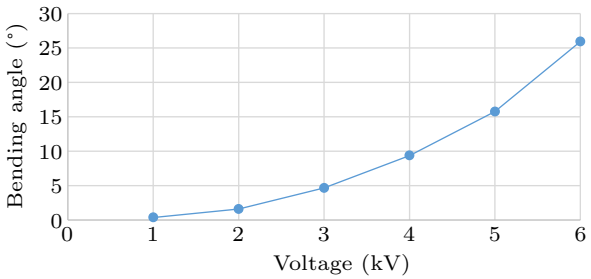


Fig. 8. Maximum bending angle of the tubular DEA with increasing applied voltage.

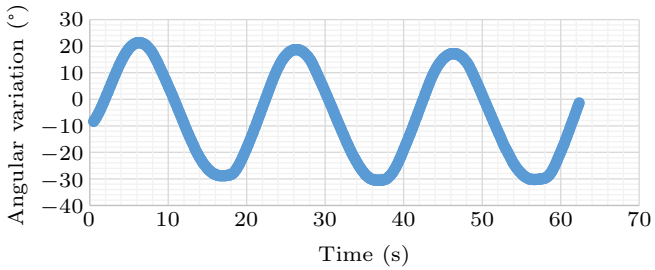


Fig. 9. The change in the bending angle of the tubular DEA over time at an applied voltage of 6.0 kV.

The relationship between the bending angle of the tubular DEA and the applied voltage is not linear and instead follows a parabolic trend. If the DE is not considered overloaded, the bending angle is expected to increase sharply with increasing applied voltage. When the voltage is 6.0 kV, the bending angle of the tubular DEA is 25.9°. The change in the bending angle of the tubular DEA over time at an applied voltage of 6.0 kV is shown in Fig. 9.

The tubular DEA bends asymmetrically from left to right, and the initial bending angle is approximately −5°. This may be due to manufacturing error, resulting in the initial bending angle of the actuator not being 0°.

4.5.2. Response characteristics

To study the response characteristics of the tubular DEA to the frequency of the voltage, a sinusoidal voltage with an amplitude of 6.0 kV and a phase difference of 180° was applied to the tubular DEA, and the bending angle of the actuator was measured. The frequencies of the sinusoidal voltage were 0.05 Hz, 0.1 Hz, 0.3 Hz, 0.5 Hz, 1.0 Hz, 2.0 Hz, 3.0 Hz, 4.0 Hz and 5.0 Hz. Figure 10 shows the bending angle of the actuator at each frequency. The gain at each frequency was calculated using the bending angle at 0.05 Hz as a reference. The gain characteristics of the tubular DEA are shown in Fig. 11.

The truncation frequency of the gain of −3 dB is approximately 0.43 Hz, which indicates that the pipe DEA has good response performance at low frequency. Therefore, the gain of the tubular DEA decreases with increasing frequency. Owing to the attenuation of the CFRP and the viscoelasticity of the elastomer material, the tubular DEA is impacted more by viscoelasticity than other types of actuators.

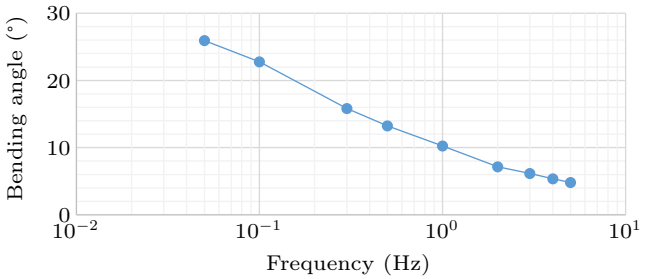


Fig. 10. Relation between the bending angle of the tubular DEA and the frequency of the applied voltage.

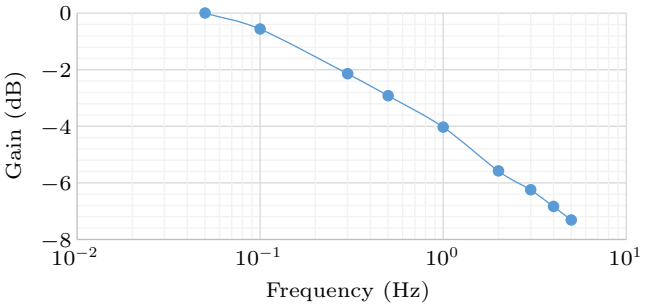


Fig. 11. Gain characteristics of the tubular DEA.

4.5.3. Driving force

Next, the driving force of the tubular DEA was measured. One end of the frame was fixed, the force measuring element was placed at the other end of the frame, and a voltage was applied to one of the electrodes. A sinusoidal voltage with an amplitude of 6.0 kV and a frequency of 0.1 Hz was then applied. A schematic diagram of the driving force measurement process is shown in Fig. 12.

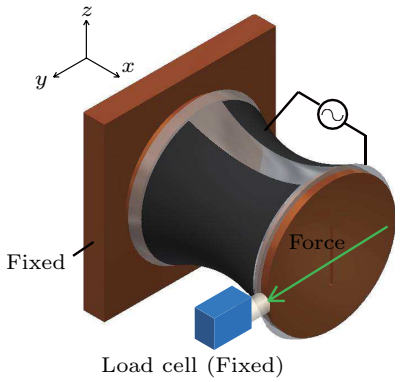


Fig. 12. Schematic diagram of the driving force measurement process.

The driving force of the tubular DEA was 73.8 mN. When the underwater robot is actually driven, this driving force is the force applied to the fluid by the robot. If the driving force is small, the robot cannot be driven to swim because of fluid resistance. Therefore, the driving force is used to propel the underwater vehicle forward.

5. Tubular driving module

The design, production and performance of the tubular driving module were studied using the tubular DEA produced in the previous section.

5.1. Design of the connection mechanism

The tubular DEA described in the previous section has good bending performance, but the performance is reduced at high frequencies. Therefore, we compensate for this reduced performance by combining multiple tubular DEAs in series in the driving module. In addition, considering the environment of the underwater robot, the driving modules are controlled separately. In particular, the fish robot can imitate special movements, such as generating traveling waves and sharp turning movements, via a dislocation driving module.

First, in the tubular DEA, the sides of the circular frame are covered with the DE material; thus, the driving module can be installed only on the top or bottom of the circular frame. When used as an underwater robot, weight affects the propulsion effect, so lightweight materials are needed. In addition, the elastomer materials can be damaged if an overly large voltage is applied. In the driving module, the best approach is to replace only the damaged parts. Therefore, a tandem mechanism is created by mounting a removable male and female structure on the circular frame. The structure of the concatenated tubular driving module is shown in Fig. 13.

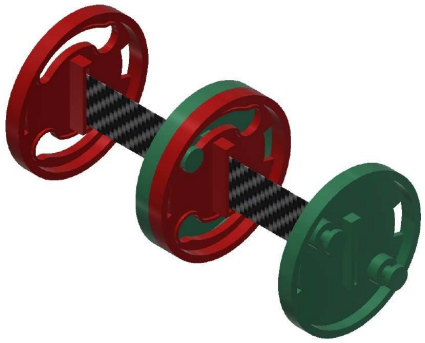


Fig. 13. The structure of the serial tubular driving module.

5.2. Evaluation of the performance of the tubular driving module

The end frame is fixed in the horizontal bending state, and the inclination of the frame is calculated according to the x and y coordinates of each section. The bending angle is calculated according to the relative angle. The series tubular driving module is shown in Fig. 14.

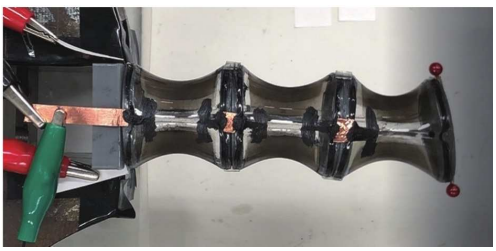


Fig. 14. Series tubular driving module.

5.2.1. Measurement of the bending angle

A sinusoidal voltage with an amplitude of 1.0–6.0 kV, a frequency of 0.05 Hz and a phase difference of 180° is applied to the tubular driving module, and the bending angle of the module is measured. Figure 15 shows the bending angle of the series tubular driving module with increasing applied voltage.

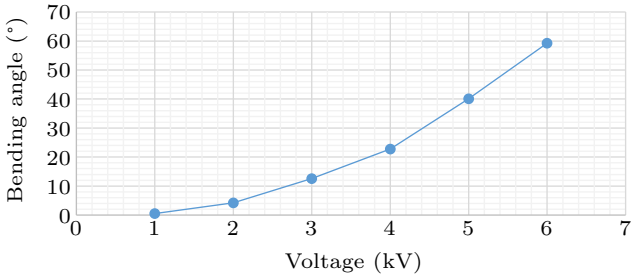


Fig. 15. The bending angle of the series tubular driving module with increasing applied voltage.

The relationship between the applied voltage and the bending angle is similar to that of the single tubular DEA, following a parabolic trend. With increasing voltage, the bending angle increases sharply. When the loading voltage is 6.0 kV, the maximum bending angle of the tubular driving module is 59.3°. The average bending angle of a single module is 19.8°, which is 76% of the bending angle of a single tubular DEA.

Then, the bending angle of each tubular driving module over time was measured at an applied voltage of 6 kV. The bending angle of each driving module changes over time, as shown in Fig. 16.

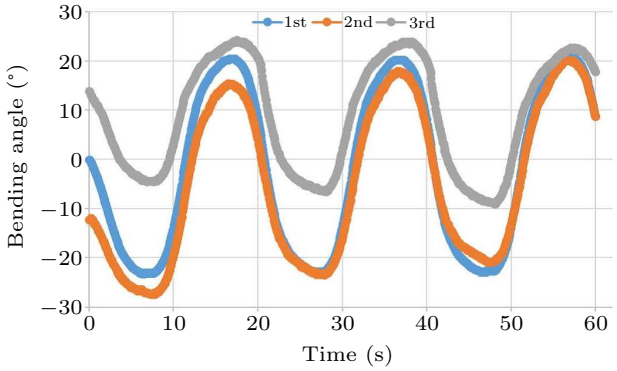


Fig. 16. Change in the bending angle of each driving module over time.

The bending angle of the third driving module is smaller, with a value of only 13.5°. If the third driving module is removed, the average bending angle of the remaining two driving modules is 22.9°, which is 88% of the bending angle of the single tubular DEA. The reason for the approximately 10% reduction is that the driving module is not strictly static and is actually subjected to inertial forces because the driving voltage frequency is 0.05 Hz.

5.2.2. Response characteristics

To study the response characteristics of the driving module to frequency, a sinusoidal voltage with an amplitude of 6.0 kV and a phase difference of 180° was applied to the tubular driving module, and the bending angle was measured. The frequencies of the sinusoidal voltage were 0.05 Hz, 0.3 Hz, 0.5 Hz, 1.0 Hz, 2.0 Hz, 3.0 Hz, 4.0 Hz and 5.0 Hz. The relationship between the bending angle of the driving module and the driving frequency is shown in Fig. 17.

In addition, the gain at each frequency was calculated on the basis of the bending angle relative to that at a frequency of 0.05 Hz. The gain characteristics of the driving module are shown in Fig. 18.

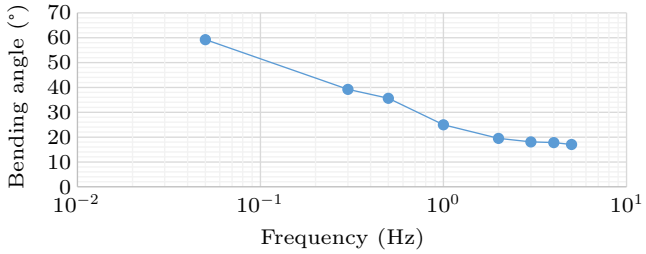


Fig. 17. Relationship between the bending angle of the driving module and the driving frequency.

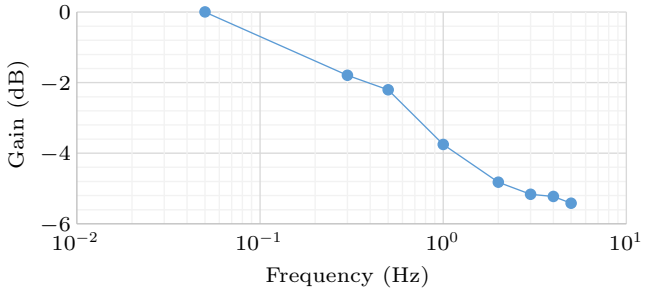


Fig. 18. Gain characteristics of the driving module.

The truncation frequency at a gain of −3 dB is approximately 0.62 Hz, which is 0.19 Hz higher than that of the single tubular DEA. Although the response is slightly better than that of the single tubular DEA, the change trend is basically the same. Therefore, as long as the problems associated with the initial bending angle of the tubular DEA can be overcome, the bending angle can be increased by using tubular DEAs in series to drive the motion of underwater robots.

6. Conclusion

In this study, a tubular actuator based on a DE has been successfully designed and manufactured, and its performance has been explored. Through detailed structural design and experimental verification, we draw the following main conclusions.

(i) Actuator design and performance optimization The tubular dielectric-elastomer actuator designed in this study

shows good bending deformation ability. By optimizing the elongation ratio of prestretching, the actuator can obtain the maximum deformation effect under voltage excitation when the axial elongation ratio is 3 times and the circumferential elongation ratio is 4 times. At a voltage of 6.0 kV, a single pipe section DEA achieves a bending angle of 25.9°, showing excellent performance.

(ii) Drive module in series to enhance performance To further improve the performance of the actuator, we designed a tubular drive module, and through a series of multiple modules accounted for the problem of performance decline at high frequency. The experimental results show that the maximum bending angle of the three tandem tube actuators reaches 59.3° under 6.0 kV, which is significantly higher than that of a single actuator. This shows that the series strategy effectively improves the overall bending performance of the actuator.

(iii) Response characteristics and driving force analysis In terms of response characteristics, the truncation frequency of a single tube type DEA is 0.43 Hz, while the truncation frequency of the drive module after the series is increased to 0.62 Hz, showing better frequency response capability. In addition, the driving force generated by the tubular DEA at 6.0 kV reached 73.8 mN, which was enough to be used as the driving force of the underwater robot to push the fluid to achieve effective swimming.

In summary, the DE tubular actuator and its drive module designed in this study have excellent performance in terms of bending angle, response characteristics and driving force, and have broad application prospects. In the future, we will further optimize the structure and materials of the actuator, explore its practical application in soft robots, underwater exploration and other fields, and contribute to the development of smart material drive technology.

Acknowledgment

Project supported by the Science and Technology Research Project of Henan Province in China (Grant No. 222102220022).

References

[1] Yu J Z, Wang C and Xie G M 2016 *IEEE Trans. Ind. Electron.* **63** 1280
[2] Zhong Y, Li Z and Du R 2018 *Adv. Rob.* **32** 25
[3] Alvarado P V and Youcef-Toumi K 2005 *J. Dyn. Sys. Meas. Control.* **128**
[4] Berlinger F, Duduta M, Gloria H, Clarke D, Nagpal R and Wood R 2018 *IEEE Int. Conf. on Robotics and Automation* 3429
[5] Nguyen D Q and Ho V A 2021 *Soft Robot.* **9** 425
[6] Katzschmann R K, DelPreto J, MacCurdy R and Rus D 2018 *Sci. Robot.* **3** aar3449
[7] Marchese A D, Onal C D and Rus D 2014 *Soft Robot.* **1** 75
[8] Wang T L, Ren Z Y, Hu W Q, Li M T and Sitti M 2021 *Sci. Adv.* **7** abf7364
[9] Pfeil S, Henke M, Katzer K, Zimmermann M and Gerlach G 2020 *Front. Robot. AI* **7** 9
[10] Xing Z, Zhang J, Mccoul D, Cui Y, Sun L and Zhao J 2020 *Soft Robot.* **7** 512
[11] Almanza M, Clavica F, Chavanne J, Moser D, Obrist D, Carrel T, Civet Y and Perriard Y 2021 *Adv. Sci.* **8** 2001974
[12] Liu C H, Lin P W, Chen J A, Lee Y T and Chang Y M 2017 *Micromachines* **8** 339
[13] Martinez T, Chavanne J, Walter A, Civet Y and Perriard Y 2021 *Smart Mater. Struct.* **30** 105024
[14] Wang S, Kaaya T and Chen Z 2020 *Smart Mater. Struct.* **29** 075037
[15] Pelrine R, Kornbluh R, Joseph J and Chiba S 1997 *Proc. IEEE 10th Annual Int. Workshop on Micro Electro Mechanical Systems*, Nagoya
[16] Yeoh O H 1990 *Rubber Chem. Technol.* **63** 792
[17] Guo Y G, Liu L W, Liu Y J and Leng J S 2021 *Adv. Intell. Syst.* **3** 2000282
[18] Chen H L and Zhou J X 2017 *The electromechanical coupling performance and applications of dielectric elastomer smart materials* (Beijing: Science Press)
[19] Carpi F, Rossi D D, Kornbluh R, Pelrine R and Sommer-Larsen P 2008 *Dielectric Elastomers as Electromechanical Transducers* (Oxford: Elsevier Ltd.)
[20] Kovacs G, Lochmatter P and Wissler M 2007 *Smart Mater. Struct.* **16** S306